Cost Optimization of Multi-Mode Train Conversion for Discontinuously Electrified Routes

Yizhe Zhang, Zhongbei Tian, Clive Roberts, Stuart Hillmansen, and Minwu Chen

***Abstract*—Rail decarbonization is a popular topic in the transportation industry. The transition from diesel-fed trains on unelectrified routes to hybrid trains or infrastructure electrification has been widely studied. However, previous studies rarely considered the installation of pantographs, fuel cells, and battery packs on multi-mode trains. This paper proposes an approach to evaluate and optimize the performance of multi-mode trains. It aims to achieve the minimum total cost, including multi-mode train conversion and route rebuilding costs, energy costs, and other maintenance costs. A simulator was developed to compute energy consumption, journey time, and onboard device replacement for multi-mode trains on discontinuously electrified routes. An evaluation has been made using the fitness function for the total cost and journey time to rank the new optimal method. A particle swarm optimization (PSO) algorithm was used to find the optimal solution. For the case study of the rebuilding plan from London St. Pancras to Leicester, before the energy price change, the optimal train costs are 34.9% less than the benchmark diesel train. After considering the future increase in energy prices, the benefits of the optimal train with low energy consumption become more significant to 40.4%.**

***Index Terms*—Multi-mode train, railway electrification, cost evaluation, optimization**

I. Introduction

The energy price for both diesel and electrified railways has been increasing annually [1]. Railways generate a large amount of greenhouse gas due to their high energy consumption. The UK government has claimed that all diesel-only trains will be removed by 2040. Electrification is a way to decrease energy consumption. Seventy per cent of the European railway network is electrified, and about 80% of trains run on an electrified route [1]. However, although only 42% of railway routes are electrified in the UK [2], the government cancelled the electrification project for the Cardiff to Swansea route, the Oxenholme to Windermere branch, and the Kettering to Nottingham and Sheffield route as part of the Midland Main Line due to financial problems [3].

This paper has been partially supported by funding of Chengdu Guojia Electrical Engineering Co., Ltd (No. NEEC-2019-B04). (Corresponding author: Zhongbei Tian.)

Y. Zhang, C. Roberts, and S. Hillmansen are with Department of Electric, Electrical and Systems Engineering, University of Birmingham, Birmingham, U.K. (e-mail: yxz372@bham.ac.uk, c.roberts.20@bham.ac.uk, s.hillmansen@bham.ac.uk).

Z. Tian is with the Department of Electrical Engineering and Electronics, University of Liverpool, Liverpool, U.K. (e-mail: Zhongbei.tian@liverpool.ac.uk).

M. Chen is with National Rail Transportation Electrification and Automation Engineering Technology Research Centre, Chengdu 611756, China and School of Electrical Engineering, Southwest Jiaotong University, Chengdu 611756, China (e-mail: chenminwu@home.swjtu.edu.cn).

Many researchers have studied electrical railway power system improvement by cutting energy consumption. Some have focused on operation strategies like energy saving by changing the regeneration strategy and using an optimal train driving strategy for actual train operation or different traction modes [4-6]. Power supply system energy control and motor traction control were considered to maximize regenerative energy and tested in reality by Iannuzzi and Tricoli [7]. System-level energy consumption evaluation has been developed and optimised using a Monte Carlo algorithm running on a DC railway power system [8, 9]. Zhang *et al.* researched an operation that supplies AC load using DC energy recovered by an inverter to save overall cost [10]. However, most tracks in the UK are discontinuously electrified due to historical and financial issues. To achieve decarbonization before 2040, the UK government has stated the operation of bi-mode trains which combine diesel and pantograph power systems. A study of discontinuous electrification evaluated the performance of different trains on the Northern Trans-Pennine route [11]. Another study of bi-mode trains and discontinuous electrification illustrated the advantages of bi-mode trains by comparing bi-mode, diesel, and pantograph operation on discontinuously electrified Great Western Main Line routes [12]. However, most electrification energy efficiency research is based on a fully electrified route, and most hybrid train research only compares the advantages of existing hybrid trains. Still, it does not further optimize the power distribution in multi-mode trains.

A new self-powered supply system powered by cleaner energy should be applied to replace diesel power during electrification gaps. Some researchers have used energy storage systems, including batteries and hydrogen fuel cells, to take the place of diesel power. A review of energy storage systems was carried out by Hannan *et al.* to present each battery and fuel cell [13]. Some studies focused on the battery pack; for example, to increase the overall energy efficiency of the railway, a battery pack is used to store regenerative energy during electrical braking [14-16]. Kleftakis and Hatziargyriou explained a novel optimization method to maximize recovered energy on a route with reversible substations and a wayside storage system. Their wayside battery pack has a simple control system, only charging and discharging between train and battery [17]. Yang *et al.* proposed a battery pack energy management strategy by adjusting the charging and discharging threshold voltage to maximize the use of the energy storage system. However, the wayside energy storage system is based on an electrified route, not well-fit discontinuous electrification [18]. The shortcoming of using a battery pack as a self-power supply system is the capacity limits.

Hybrid trains combining a battery pack and other power supply systems such as fuel cells can overcome the capacity limit problem [19-23]. A hybrid vehicle model simulator has been developed by Gao using the Powertrain System Analysis Toolkit (PSAT) and Advanced VehIcle SimulatOR (ADVISOR) based on experiential models [24]. A feasibility study for a hybrid train showed a comparison between a fuel cell energy supply system combined with an ultra-capacitor and a Li-ion battery but without considering regeneration [25]. An optimal control strategy for a fuel cell/supercapacitor hybrid tramway has been used to reduce hydrogen consumption [26] further. Torreglosa *et al.* tried to add a hydrogen fuel cell to the Urbos 3 tramways, operating in Spain to save energy [27]. That research on energy storage systems did not consider a combination

with electrification, which has much higher energy efficiency; doing so could further decrease the energy cost. Hence, the battery is only a tool to save regenerative energy without connecting with the overhead line.

Most previous studies have not considered the combination and distribution of those novel power supply systems and train operation in hybrid train research. When discussing train conversion, most researchers think only about the capability of the power system but not the conversion cost. This paper aims to demonstrate a financially effective plan for converting diesel engine trains and route electrification during an operation period. Three different kinds of energy supply systems are combined as the new supply system to power trains on discontinuously electrified routes. The highlights of this paper are as follows:

- Multi-mode train powered by pantograph, hydrogen and battery simulator is developed.
- The dynamic battery pack model is controlled by its state and train performance.
- Multi-energy usage is optimized by a specific energy management strategy.
- The cost model includes initial financial cost and further operation cost.
- An adaptive particle swarm optimization is used to find the optimal cost solution.

The structure of this paper is organized as follows: Section I explains the current situation of changes to railway energy supply methods. Section II shows train supply systems and operation management. Section III presents the methodology for evaluating the plan using the cost function and an improved PSO algorithm. Section IV demonstrates a case study of the rebuilding plan for the route from London St. Pancras to Leicester and train conversion. An existing diesel train is compared with converted trains in different electrification scenarios. Estimated energy price changes are considered to forecast the effect of rising energy prices on the simulation results.

II. Energy Supply System Distribution

A. Multi-Mode Energy Flow

Most rail lines are partly electrified in the UK. On discontinuously electrified routes, the power supply is divided into two parts: overhead line power to the motor as the main or only supply system on the electrified part, and a self-powered traction system such as hydrogen fuel cells and battery pack, to supply power to the motor together, on the non-electrified part. Making the best use of electrification is an effective way to save energy costs, and a self-powered traction system is also necessary when no overhead line is accessible. A train traction system powered by a multi-mode power system is applied in this situation. The hydrogen fuel cell (HFC) train can operate on the track regardless of the discontinuous electrification. Similar to diesel train, HFC train consumes fuel to drag them. The onboard hydrogen fuel cell can produce electricity by consuming hydrogen. The electricity can be sent to the motor, converted to kinetic energy.

Train traction movement depends on Newtonian motion equations as equation (1).

$$m(1+\lambda)a = \mathrm{F}_{\mathrm{tra}} - mgsin(\alpha) - \mathrm{F}_{\mathrm{res}} - F_{bra} \qquad (1)$$

$$F_{res} = (A + Bv + Cv^2) \quad (2)$$

where m is the mass of the train and a is train acceleration/deceleration rate. The inertial effect, also called the rotary allowance, $\lambda = 8\%$, and α is the angle of the slope. The resultant force consists of the traction force F_{tra}, gravity force mg in the direction of movement, and resistance according to the Davis equation, where A, B, and C are the Davis equation constants; v is the operation velocity. The braking force F_{bra} is produced by the combination of electrical braking and mechanical braking. Traction power is supplied by the motor powered by a multi-mode power system, and the effort is inversely proportional to velocity.

$$F_{tra} = \eta_{train} \times (P_{demand}/v) \quad (3)$$

$$P_{demand} = P_{Pan} + P_{FC} + P_{BP\_disch} \quad (4)$$

$$F_{bra} = P_{bra}/v \quad (5)$$

where η_{train} is the efficiency of the train set as 85% typically, and P_{Pan}, P_{FC}, and P_{BP_disch} are the output power of the pantograph, hydrogen fuel cell, and battery pack, respectively. The sum of power supply system is equal to the power demand of traction motor P_{demand}. The braking force F_{bra} depends on the braking power and its operating speed.

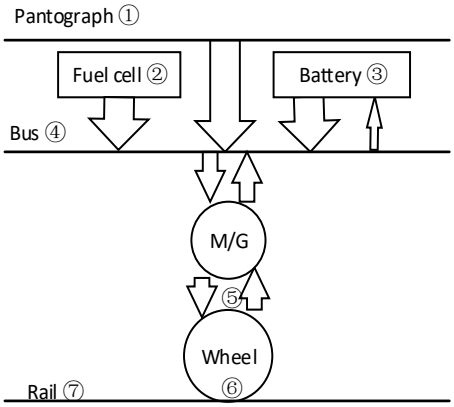

Fig. 1. Energy flow

Seven kinds of energy flow inside the trains are shown in Fig. 1. Energy from the pantograph ①, fuel cell ②, and battery pack ③ connect to the power bus ④. Electrical energy on the power bus ④ is converted into mechanical energy ⑤ by the motor and sent to the wheels through the gearbox to push the train forward. When the train is braking, kinetic energy ⑥ and potential energy ⑦ are regenerated to electricity and sent back to the power bus ④. Any electricity on the power bus which is not consumed can charge the battery pack ③.

In equation (6), the energy consumption from each source integrates the power supplied by different systems. In this paper, the battery pack energy consumption ΔE_{BP} will be charged through a transmission line. When considering the use of battery pack energy, the difference in the energy remaining in the battery pack in kWh is given by equation (7).

$$\begin{cases} E_{\mathrm{Hy\_C}} = \dfrac{\int P_{FC}\,dt}{\eta_{FC}} \\ E_{\mathrm{Ele\_C}} = \dfrac{\int P_{Pan}\,dt + \Delta E_{BP}/\eta_{BP}}{\eta_{\mathrm{Pan}}} \end{cases} \tag{6}$$

$$\Delta E_{BP} = \left(SOC_{fin} - SOC_{ini}\right) \times Capa_{BP} \tag{7}$$

where $E_{\mathrm{Hy\_C}}$ and $E_{\mathrm{Ele\_C}}$ represent hydrogen and electrical energy consumption; η_{FC} and η_{Pan} are the energy efficiency of the hydrogen fuel cell and pantograph before injection to trains; η_{BP} is the battery pack efficiency; and $Capa_{BP}$ is the battery pack capacity. SOC_{fin} and SOC_{ini} are the battery state of charge when the train arrives at the terminal station and departs from the start station, respectively.

B. Traction Simulation

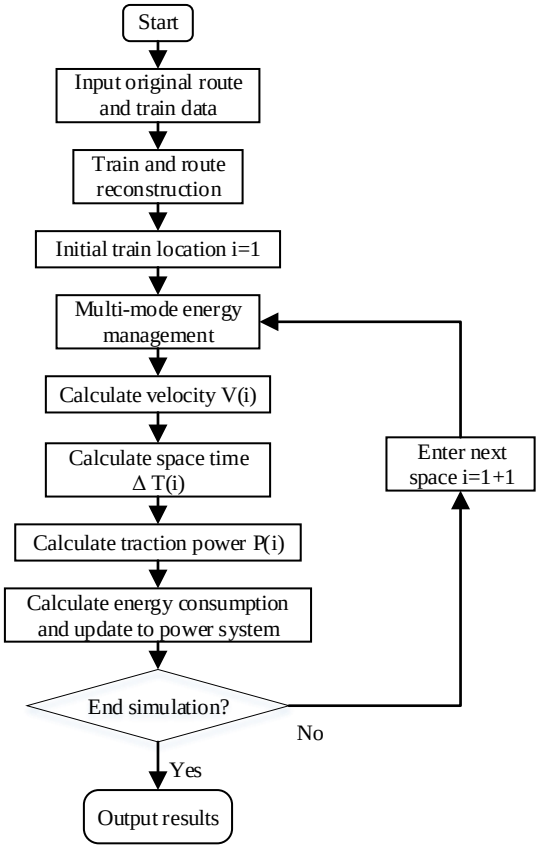

Fig. 2. Simulator flow chart

Traction simulation simulates the movement of trains by traction and the power system over the whole route. In the first two steps of Fig. 2, train and route reconstruction are sent to the simulator to represent upgrading the original train and route. Train reconstruction considers converting a diesel train to a multi-mode train using hydrogen fuel cell power and battery power, and route reconstruction considers extending the length of electrified track. For the loop to calculate train traction,

this simulator is computed based on the distance domain (discretization distance space ΔD). At the beginning of each space, the power system status is the same as that at the end of the previous space. As equation (8) shows, train velocity at the end of discretization space $V(i)$ is calculated according to the acceleration/deceleration rate in equation (1) and the end velocity of previous space $V(i-1)$. Time consumed $\Delta T(i)$ in any space is calculated by the average velocity in each step *i*:

$$V(i) = \sqrt{V(i-1)^2 + 2 \times a \times \Delta D} \qquad (8)$$

$$\Delta T(i) = \frac{2 \times \Delta D}{V(i-1) + V(i)} \qquad (9)$$

Then, all energy consumption in the current space *i* can be determined and updated to the power systems; the status at the end of step is determined and set as the start status of the next step *i*+1. Once that has been completed for all spaces (whole journey), the completed performance of train operation can be shown.

C. Energy Management Strategy

The use of the multi-mode energy source is controlled by the energy management system. This paper identifies four driving scenarios according to differences in train operation and route electrification. A default management strategy is set to cover these driving scenarios, as shown in Fig. 3.

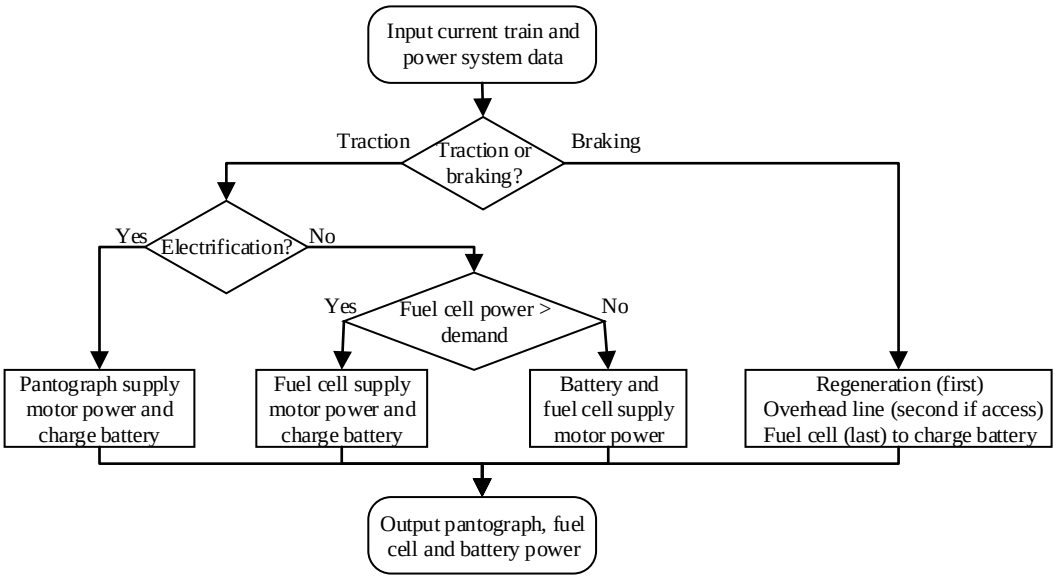

Fig. 3. Flow chart for the energy management system

1) Traction on Electrified Route

On an electrified route, the overhead line can supply all the power needed by the motor and battery pack. Because of the highly high-power supply, the battery pack is always charged at its maximum charging power on electrified routes.

2) Traction on Non-Electrified Route with Low Power Demand

Less traction power is demanded if the train is operating in a low-speed acceleration stage or a low traction-force stage like cruising or going downhill. The fuel cell can charge the battery pack if motor power demand P_{demand} is below the fuel cell maximum power $P_{FC\ MAX}$ as shown in equation (10).

$$P_{BP\_ch} = P_{FC\ MAX} - P_{demand} \tag{10}$$

where P_{BP_ch} is the charging power of the battery pack.

3) Traction on Non-Electrified Route with High Power Demand

When the train operates in high power demand situations such as high speed or high traction force, if the installed fuel cell does not have high output power, it no longer meets the power demand. The maximum power $P_{FC\ MAX}$ is sent to the power bus, and the battery pack is discharged to compensate for the power demand as given by equation (11). The battery pack stops discharging when the state of charge (SOC) is below the low operation limit. The ΔE_{BP} in equation (7) is the battery pack energy changes. It should also be equal to the sum of battery pack discharging power P_{BP_disch} minus the sum of battery pack charging power P_{BP_ch} after considering the battery pack efficiency.

$$P_{BP\_disch} = P_{demand} - P_{FC\ MAX} \tag{11}$$

$$\Delta E_{BP} = \frac{\int P_{BP\_disch}\, dt}{\eta_{BP}} - \eta_{BP} \times \int P_{BP\_ch}\, dt \tag{12}$$

Overall, on a non-electrified route, the hydrogen fuel cell is the primary power supply system, whereas the battery pack only compensates for peak power demand.

4) Braking Stage

At the braking stage, the regenerative braking and non-regenerative braking work simultaneously. When the train operates electrical braking, the generator regenerates high power to charge the battery through the power bus. The resting power that cannot transfer to the power saving in the battery pack is consumed by non-regenerative brakings, such as disc braking. Regenerative power from the generator has the highest charging priority. If the regenerative power is not as high as battery maximum charging power, the overhead line electricity charges the battery to compensate for the charging power. But if the train is braking in non-electrification part, the fuel cell charges battery by taking the overhead line. In this paper, the combination braking power P_{bra} is always set as its maximum value, as equation (13) shows. For each kind of train, the braking power, braking force, and deceleration have their cap value (maximum value), respectively.

$$P_{bra} = P_{regen} + P_{non-regen} \tag{13}$$

$$\begin{aligned} P_{bra} &\le P_{bra\,max} \\ F_{bra} &\le F_{bra\,max} \end{aligned} \tag{14}$$

$$a_{bra} \leq a_{bra_{max}}$$

III. METHODOLOGY

A. Cost Calculation

The total cost C_{total} can be separated into three different parts: initial cost C_{ini}, energy cost C_e, and replacement cost C_{rep} as shown in equation (15).

$$C_{total} = C_{ini} + C_e + C_{rep} \quad (15)$$

1) Initial Cost

Initial cost includes train conversion cost C_{conv} and route rebuilding cost $C_{route\ reb}$, as shown in equation (16).

$$C_{ini} = C_{conv} + C_{route\ reb} \quad (16)$$

C_{conv} as shown in equation (17) includes the essential fixed rebuilding cost C_{fixed} which includes the cost of the motor, circuit, converter, and other components, and the cost of the battery pack and its associated components C_{BP}, as well as fuel cell cost C_{FC} and hydrogen tank cost C_{Hy_t}. Besides, the number of converted trains are counted as N_{trains}. Equation (18) shows two different parts of $C_{route\ reb}$. Normal route cost C_{normal} includes electrification infrastructure and the cost of refurbishing the route from the ends of the electrified part to the terminal station except for tunnels. Tunnel electrification cost is calculated separately as C_{tunnel} because it is much higher due to the complications of rebuilding tunnels or bridges compared with regular routes.

$$C_{conv} = N_{trains} \times (C_{fixed} + C_{BP} + C_{FC} + C_{Hy\_t}) \quad (17)$$

$$C_{route\ reb} = C_{normal} + C_{tunnel} \quad (18)$$

2) Energy Cost

Diesel train and multi-mode train energy costs are calculated in equations (19) and equation (20) separately. For diesel trains, the energy cost $C_{e_{diesel}}$ only includes diesel consumption according to diesel fuel price Pr_D, engine power P_{Engine} and its efficiency η_{Engine}, whereas the cost for a multi-mode train considers both hydrogens $E_{\mathrm{Hy\_C}}$ and electricity $E_{\mathrm{Ele\_C}}$ energy consumption multiplied by their price $\mathrm{Pr_H}$ and $\mathrm{Pr_E}$, respectively. Supposing the energy price Pr changes annually and the price change slope a is same as that in recent decades, the fuel price in the j-th year is shown in equation (21). assuming all trains run as planned by using N_{annu} fuel each year, the total cost C_β of energy β (either diesel, hydrogen, or electricity) in the 40 years is given by equation (22).

$$C_{e_{diesel}} = Pr_D \times \frac{\int P_{Engine} dt}{\eta_{Engine}} \quad (19)$$

$$C_{e_{multi-mode}} = \mathrm{Pr_H} \times E_{\mathrm{Hy\_C}} + \mathrm{Pr_E} \times E_{\mathrm{Ele\_C}} \quad (20)$$

$$Pr_\beta(j) = Pr_\beta(i) \times (1 + j \times a) \quad (21)$$

$$\mathrm{C}_\beta = N_{annu} \times \sum_{j=1}^{40} Pr_\beta(j) \quad (22)$$

3) Replacement Cost

Usually, all equipment has an estimated life cycle. On reaching the end of its lifespan, it should be replaced. In this paper, the battery pack $C_{BP\,rep}$, fuel cell system $C_{FC\,rep}$, and traction system equipment $C_{motor\,rep}$ are considered, and their costs are summed as C_{rep} in equation (23). The battery pack need to be replaced due to its degradation. Every time it charges or discharges, the degradation effect of the materials would reduce the battery capacity [28]. If the maximum capacity decreased to approximately 75%, it would be considered failed [29]. In this paper, the measurement of battery usage is the depth of discharge. The sum of all state of charge changes due to energy discharging is counted as the total depth of discharge. The replacement of the battery pack is determined according to the times of its lifespan depth of discharge $DOD_{lifespan}$ and total depth of discharge as in equation (24). However, the replacement period for the fuel cell and the motor is assumed as a fixed period of years as $year_{FC\,period}$ and $year_{motor\,period}$ in equation (25) and equation (26). Except for the replacement cost, the first-time system installation cost is included in C_{conv}.

$$C_{rep} = C_{BP\,rep} + C_{FC\,rep} + C_{motor\,rep} \quad (23)$$

$$C_{BP\,rep} = C_{BP} \times \left(\frac{\int \frac{P_{BP_{disch}}}{Capa_{BP}}}{DOD_{lifespan}} - 1\right) \quad (24)$$

$$C_{FC\,rep} = C_{FC} \times \left(\frac{year_{total}}{year_{FC\,period}} - 1\right) \quad (25)$$

$$C_{motor\,rep} = C_{fixed} \times \left(\frac{year_{total}}{year_{motor\,period}} - 1\right) \quad (26)$$

B. Optimization Algorithm

PSO is an optimization algorithm attributed to Kennedy, Eberhart, and Shi to simulate birds' movement [30]. Hu has used adaptive PSO with multiple adaptive methods (MAM) and Son based on a kernel support vector machine to improve its convergence speed and exploration capability [31, 32]. This paper discovers the optimal result by a simple adaptive PSO. Fig. 4 shows the flow chart of optimization. The details of train simulator and fitness function block are shown in Fig. 6.

Step 1: A set of railway rebuilding plans with variables initialized by random values and related modelling data are input to the optimization program.

Step 2: Those railway rebuilding plans are simulated based on a railway route and evaluated by the fitness function.

Step 3: The results are ranked according to their fitness value, and the overall best plan and individual best plan are recorded.

Step 4: If the overall best plan meets the stop condition, it will be sent to Step 6. Otherwise, all plans are forward to Step 5.

Step 5: All plans need to be updated according to PSO's updating method. Besides, new plans out of the variables range need to be adjusted and then sent back to Step 2 with those plans located inside the range.

Step 6: Output the best plan.

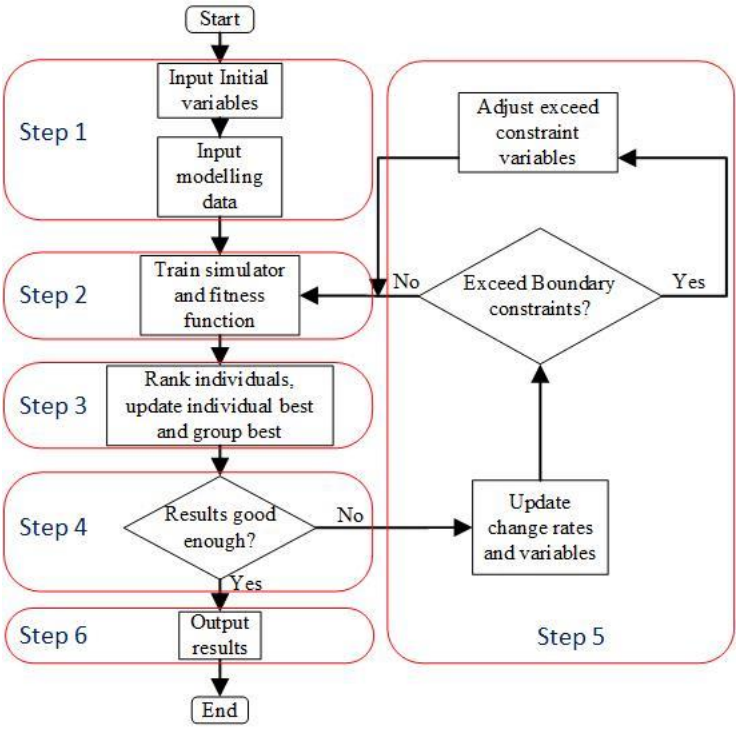

Fig. 4. Flow chart of the optimization

1) Optimization Variables

The optimal variables in this paper are battery pack power P_{BP}, hydrogen fuel cell power P_{FC}, new electrified regular route length L_{NE}And new electrified tunnel length L_{TE}. In these four variables, P_{BP} and P_{FC} present the trains conversion. They represent the new train power distribution in battery packs and hydrogen fuel cells. L_{NE} and L_{TE} are related to route rebuilding. The route rebuilding has a considerable cost impact due to its high infrastructure fees. Besides, a more extended electrification section means the train can get more high-efficient, high-power overhear wire electricity. That can influence trains operation performance with the different design of other two variable factors. Hence, the energy cost is finally different.

Regarding the route rebuilding variables, it is supposed that part 1 is currently the existed electrified route, whereas Part 2 to Part 8 is not electrified, as Fig. 5 shows. When a train operates on an existing and newly electrified route, it can gain energy from an overhead line. Because electrification projects typically extend from the current electrified route, new electrification starts from the present electrified part to the terminal. In this optimization, the length of the yellow part is to

be optimized. These parts are electrified, including the regular route of Part 2, Part 4, and Part 7 and tunnels of Part 3 and Part 5. Part 6 tunnel and Part 8 usual route remain unelectrified.

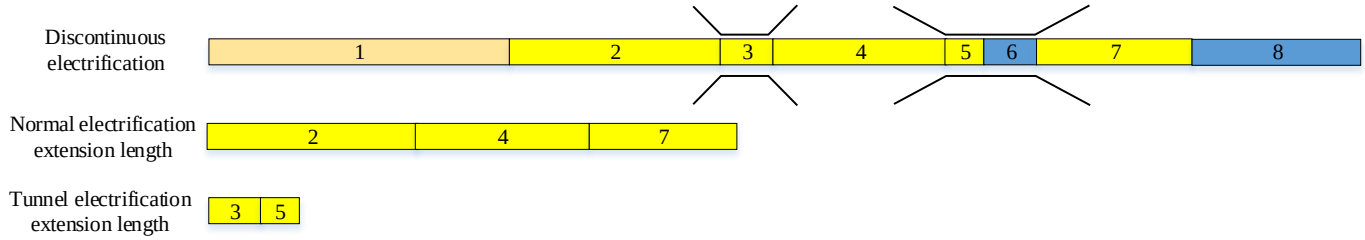

Fig. 5. Electrification variables

2) Fitness Function and stops condition

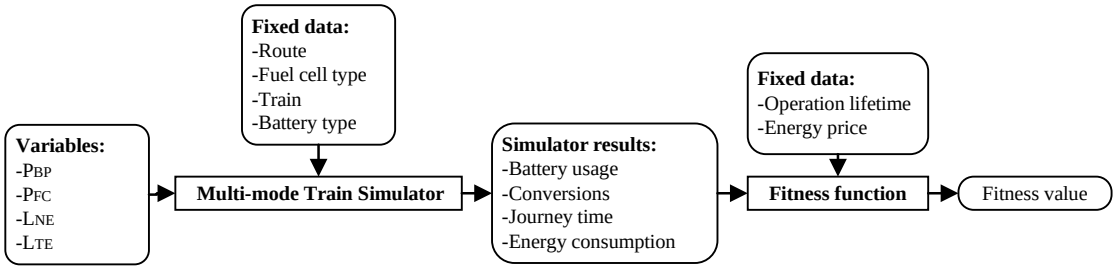

Fig. 6. Calculation of fitness value

The evaluation method combines a multi-mode train simulator and a fitness function block. Fig. 6 shows the contents of the input and output of the evaluation. The block of multi-mode train simulator detail is shown in Fig. 2. Equation (27) gives the fitness function, including the total cost and the journey time factor (TF). The total cost is the spent money on conversion, rebuilding, and future operation cost in the unit of GBP. Besides, the time factor TF shows the profit or penalty due to journey time difference in equation (28) with the same unit of GBP. If the journey time T_j exceeds the maximum time limit T_{target}, a time penalty is applied. However, the time profit is varied according to the optimization requirement. If the optimization recommends reducing journey time, the κ_{profit} is negative and set as a greater absolute value. For those optimizations which requiring no obvious journey time changes, the κ_{profit} can set as 0 or positive.

$$f(P_{BP}, P_{FC}, L_{NE}, L_{TE}) = TF + C_{total} \tag{27}$$

$$TF = \begin{cases} \kappa_{profit} \times (T_j - T_{target}) & if\ T_j < T_{target} \\ \kappa_{penalty} \times (T_j - T_{target}) & if\ T_j > T_{target} \end{cases} \tag{28}$$

where T_{target} is the target journey time; κ_{profit} is the time profit coefficient for earliness and $\kappa_{penalty}$ is the time penalty coefficient for tardiness. It takes more time to recharge the battery pack to its initial state if the final SOC of the battery pack is lower than the initial state. That extra time is also considered as journey time except for operation time T_{op}.

$$T_j = T_{op} + \frac{\Delta E_{BP}}{P_{BP\_ch}} \tag{29}$$

Determining the optimal plan found condition depends on the best fitness value changes. If the best fitness value changes rate $CR_{fitness}$ over several iterations is less than a convergence coefficient, the optimization program can be stopped.

$$CR_{fitness} = \frac{f_{new\ best} - f_{old\ best}}{f_{old\ best}} \tag{30}$$

3) Optimization Variables Update

The primary variable optimization principle is demonstrated in Fig. 7. Updating of the variables' change rate in each iteration as shown in equation (31) and equation (32) depends on the last change rate inertia $\omega\overrightarrow{V_{(\iota)}^{(n)}}$, cognitive component $c_1 \times r_1 \times \left(\overrightarrow{X_{\iota best}^{n}} - \overrightarrow{X_{\iota}^{n}}\right)$, and social component $c_2 \times r_2 \times \left(\overrightarrow{X_{g best}} - \overrightarrow{X_{\iota}^{n}}\right)$ which are related by the difference to the individual best point $\overrightarrow{X_{\iota best}^{n}}$ and group best point $\overrightarrow{X_{g best}}$ respectively.

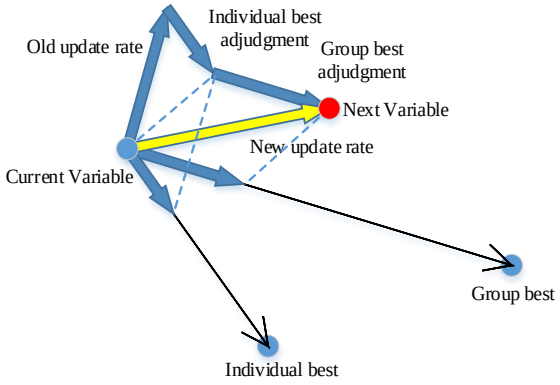

Fig. 7. Individual update

$$\overrightarrow{V_{(\iota+1)}^{(n)}} = \omega\overrightarrow{V_{(\iota)}^{(n)}} + c_1 \times r_1 \times \left(\overrightarrow{X_{\iota best}^{n}} - \overrightarrow{X_{\iota}^{n}}\right) + c_2 \times r_2 \times \left(\overrightarrow{X_{\iota best}} - \overrightarrow{X_{\iota}^{n}}\right) \tag{31}$$

$$\overrightarrow{X_{\iota+1}^{n}} = \overrightarrow{X_{\iota}^{n}} + \overrightarrow{V_{\iota}^{n}} \times 1 \tag{32}$$

4) Constraints and adjustment

As the optimizing variables, the four variables ($P_{BP}, P_{FC}, L_{NE}, L_{TE}$) have their constraints. The minimum value of each variable is set as 0, whereas the maximum constraint of the battery pack is 1000 kW and that of the hydrogen fuel cell is 2240 kW; the regular route and tunnel rebuilding lengths are set as the length of the simulated unelectrified route. If the updated plan variables exceed the constraints, the value of the variable $\overrightarrow{X_{\iota+1}^{n}}$ will be set as the edge (maximum or minimum) value and the variables change rate $\overrightarrow{V_{\iota+1}^{n}}'$ is opposite to avoid exceeding the constraint again.

$$\overrightarrow{V_{i+1}^{n}}' = -\overrightarrow{V_{i+1}^{n}} \quad (33)$$

IV. Case Study

A. Simulation Data

1) Route Selection

The selected simulation route is from London St. Pancras to Leicester (158.54 km), part of the Midland Main Line, with six intermediate stations, as shown in Fig. 8. The black line shows line speed restrictions. The first half of the route, with 79.46 km from London St. Pancras station to Bedford station, is electrified. Besides that, there are 11 tunnels located on the rest of the route, which is not electrified [33, 34]. A two-direction operation is considered to obtain more accurate optimization results; from the start station, trains operate to the terminal station and then run back.

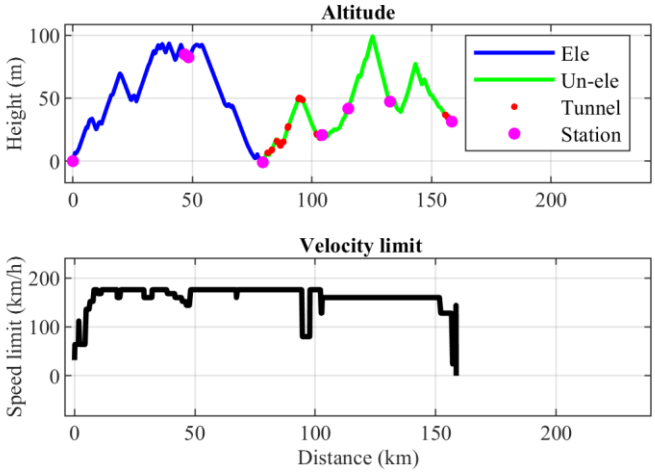

Fig. 8. Line altitude, stations and speed limit from St. Pancras to Leicester [33]

2) Battery Characteristics

TABLE I

Simulation Battery Pack Characteristics

Objectives	**Value**	
Working SOC range	**lowest**	0.1
	highest	1
Discharging rate	5C	
Charging rate	**CC**	2C
	CV	0.1C

The battery used in this paper is the $LiFeO_4$ battery. As TABLE I shows, the battery has its working SOC range. The maximum discharging power is the optimizing variable in the discharge mode, and its capacity depends on that power. When the SOC is below 0.93, the constant current (CC) charging mode is active during charging. Once the SOC is above the threshold, the charging mode is switched to a constant voltage charging mode[35, 36].

3) Train Conversion Design

TABLE II

TRAIN CONVERSION CHARACTERISTICS

Objectives	Value
Overhead line energy efficiency	87%
Hydrogen fuel cell efficiency	Varied
Diesel engine efficiency	30%
Battery charging/discharging efficiency	94%
Diesel engine system	6.78 tonnes/car
Electrical motor system	4 tonnes/train
Battery pack system	20 kg/kW
Fuel cell system	7.2 kg/kW
Hydrogen tank (350 Pa)	0.66 kg/kWh

The average train lifetime of 40 years is applied as the simulation time range; 12 Class 222 diesel trains are assumed to be converted, and four cars are included in each train. The energy efficiency depends on the power supply system used as an energy source for the motor. The most efficient supply system is the overhead line (87%), whereas the diesel engine efficiency is lowest at 30%. At the same time, supposing the hydrogen fuel cell efficiency is not fixed at its maximum value. The efficiency from converting hydrogen to electricity is varied, and it is a function of its output power. According to the research by Qi Li, the efficiency keeps rising to around 52%, which is the peak efficiency during the output power increased to 20 kW. And it is almost linearly decreasing if the output power gets higher, to 45% once output power reaches its maximum power of 100 kW [26]. The efficiency curve can be roughly plotted as Fig. 9.

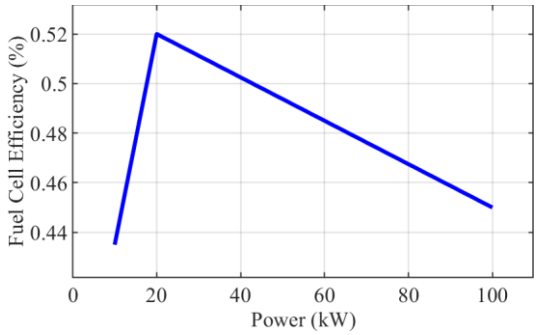

Fig. 9. Hydrogen fuel cell efficiency vs fuel cell output power

It is assumed that the train weight will change when considering train conversion design. There is a fixed weight change when considering diesel train to electric train, whereas the power system weight is varied depending on its designed capacity or power [20, 22]. Those system power-weight ratio data is from the HydroFLEX 1.1 project at the University of Birmingham. HydroFLEX is the UK's first hydrogen fuel cell-powered train, which was already mainline tested in 2019.

4) Data for Cost Calculation

TABLE III

PRICE OF DIFFERENT OBJECTIVES

Objectives	Price
Fixed cost	£40k/car
Battery system	£217/kWh
Fuel cell system	£43/kW
Hydrogen tank	£8/kWh
Normal route electrification	£1.8 M/ptk
Tunnel electrification	£7.5 M/ptk
Diesel fuel	£0.13/kWh
Hydrogen fuel	£0.3/kWh
Electricity	£0.1/kWh

The price of train conversion, route rebuilding and fuel are listed in TABLE III. Like train weight, the train conversion cost varies according to power system design. The route rebuilding cost is counted as its length, and there are two rebuilt tracks in each line [37]. The replacement period is variable depending on the equipment type. The lifespan of the battery pack is 3000 full-depth charges. A new hydrogen fuel cell needs to be installed on a train every 40 years. The hydrogen fuel tank should be replaced every 20 years [22, 35, 38, 39]. The κ_{profit} in this paper is 0 because this study aims to find an optimal plan without much journey time changes, at the same time, the $\kappa_{penalty}$ is set as £40 per minute delay[40, 41].

B. Single-Mode Train Results

TABLE IV

SINGLE-MODE TRAIN AND ROUTE DESIGN PLANS, ENERGY CONSUMPTION, AND COST

Train/route plan	Weight [tonnes]	Diesel engine power [kW]	P_{BP} [kW]	P_{FC} [kW]	L_{NE} [km]	L_{TE} [km]	Journey time [s]	Traction energy consumption [kWh]	Fuel energy cost [£]	Energy cost saving
Benchmark diesel train	214	2240	0	0	0	0	9340.3	2190.6	1116.8	0
Hydrogen train	215.38	0	0	2240	0	0	9346.3	2196.1	1682.4	−50.6%
Full electrification (except tunnels)	190.88	0	0	0	76.11	0	9135.2	2134.6	288.65	74.15%
Full electrification	190.88	0	0	0	76.11	2.97	9116.2	2137.4	289.03	74.12%

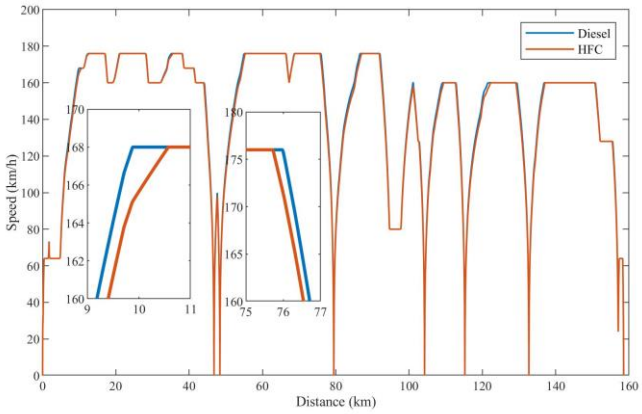

Fig. 10. Diesel and HFC train velocity curve from St. Pancras to Leicester

Details for single-mode trains each run are shown in TABLE IV. It offers the different parameters related to those optimized variables and the performance of single-mode trains, including diesel, hydrogen fuel cell, and electric train on full electrification with and without tunnel electrification. There is almost the same performance for diesel and hydrogen fuel cell trains but still some differences. It shows that the hydrogen fuel cell train has a journey time of 6 s (0.06%) longer than the diesel train. Furthermore, the difference in traction energy is 0.25%, less than the 0.64%which is the weight difference. More traction energy is consumed by a hydrogen train, even though better transfer efficiency contributes to 48.67% less fuel energy consumption than for a diesel train. Although the price of hydrogen per kWh is 2.3 times that of diesel, the hydrogen train energy cost for each run is 50.6% higher than for the diesel train. From Fig. 10, at any location, the speed of the diesel train is higher than that of the hydrogen train. That is because diesel trains can faster change their speed no matter acceleration or deceleration, with the same maximum power supply. When the train is at the acceleration stage, the hydrogen train reaches its power cap before the diesel train, and then its acceleration becomes lower due to no higher power supported.

The average velocity for both electrification scenarios is higher than for the benchmark diesel train. This is mainly because the electric train is lighter than the others and has greater acceleration power. These two energy costs are nearly the same, a saving of around 74% compared with the benchmark diesel train. TABLE IV also shows that more traction energy is consumed by a hydrogen train than any pantograph train. Broadly speaking, this is due to a hydrogen train being heavier than other trains, so it needs more energy to drag it forward. In detail, this paper considers three operation stages during the journey: acceleration, cruising, and braking. The traction energy consumed by the diesel and pantograph trains is obviously less than for the fuel cell train. Those lighter trains speed up to maximum velocity earlier and enter the cruising stage, demanding less power. However, qualitative analysis is hard to compare the energy consumption during the entire cruising stage. On the one hand, the hydrogen fuel cell train has a shorter cruising time than the diesel train. On the other hand, as said above, the power demand for the fuel cell train in the cruising stage is higher than for others.

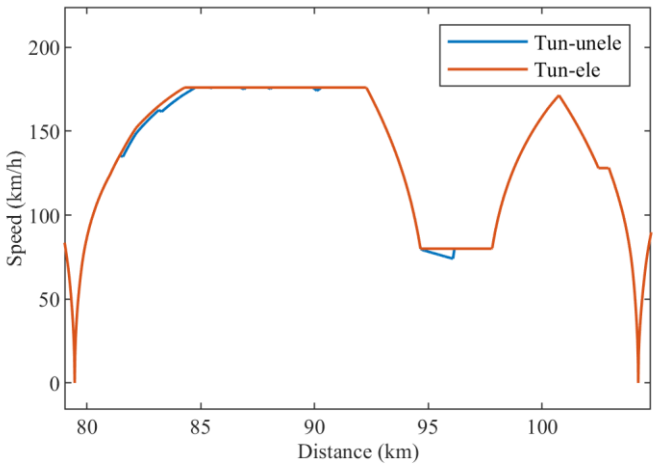

Fig. 11. Velocity of pantograph trains on the fully electrified route (with or without tunnel electrification) between Bedford and Wellingborough

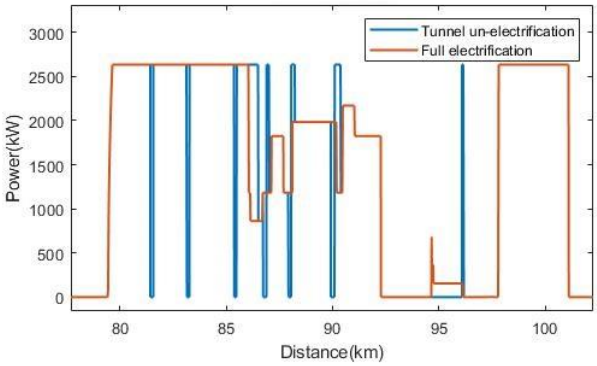

Fig. 12. Overhead line power of pantograph trains on the electrified route between Bedford and Wellingborough

The speed differences between the two electrification scenarios are due to energy support in tunnels. There are nine tunnels located between Bedford and Wellingborough. The train should be in traction mode in the first seven tunnels and braking mode in the other two tunnels before Wellingborough. Velocity drops in unelectrified tunnels can be seen in Fig. 11. However, their drops are not apparent. The most significant reduction inside a tunnel is in the Sharnbrook Tunnel, the seventh tunnel where speed decreases by 6 km/h, from 80km/h to 74 km/h. Those tiny drops in speed make the journey time in the non-electrified tunnels scenario slightly longer than for the electrified tunnels scenario, by less than 19 s in TABLE IV. Due to speed drops in tunnels, after leaving the unelectrified tunnel and connecting with an overhead line, the train gains maximum power instead of balanced cruising power in Fig. 12 and then speeds up to the balance speed as shown in Fig. 11.

C. Optimal Multi-Mode Train

Fig. 13 shows the velocity curve of the optimal train for a two-direction run. According to the result optimized by adaptive PSO, the optimal train has an 800 kW battery pack installed onboard without any hydrogen fuel cell. Besides that, the electrification of the regular route is extended for another 53.35 km before Market Harborough without any extra electrification for the tunnels. At the beginning of the electrified route, the battery pack starts charging from the overhead line from a SOC of 20%, the initial SOC, and it releases energy in the non-electrified tunnels to keep the traction system in operation in Fig. 14. The route is still unelectrified between Market Harborough and Leicester. There is a self-traction system

on the train to run back using the fuel cell and battery pack. The final journey time is 9340 s, the same as the diesel train. The train operation is not getting slower because the delay penalty is too high, and the energy cost saving cannot cover the time penalty.

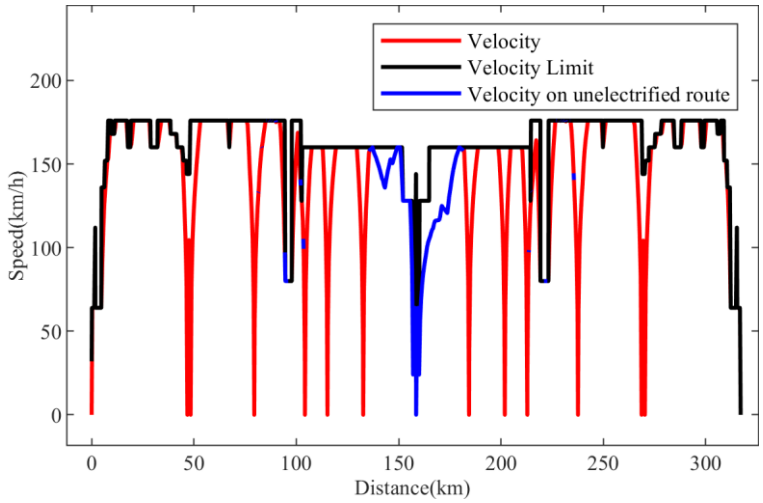

Fig. 13. The velocity of the optimal train in up and down directions

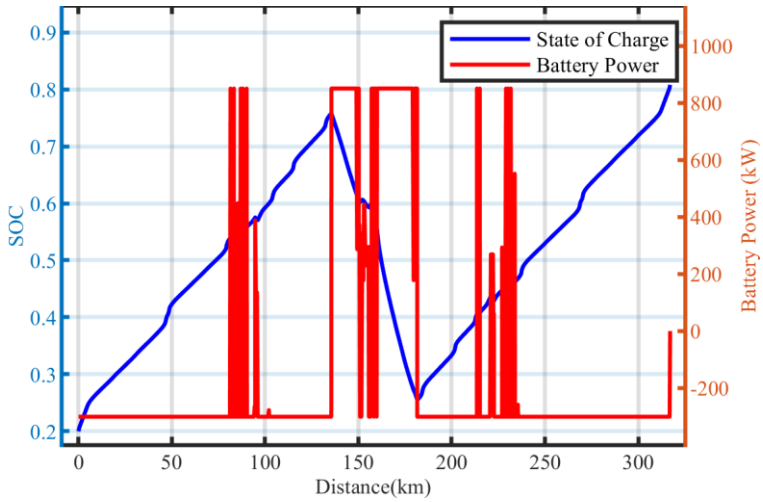

Fig. 14. Optimal train battery pack SOC

Due to no fuel cell installation, the optimal train only spends battery and overhead line energy on traction. From Fig. 14 and Fig. 15, it can be seen that the battery pack is charging in a constant voltage charging stage during the whole trip as its SOC has never been over 93%. Inside the tunnel between Bedford and Market Harborough, the traction system uses the battery pack to provide energy even though there is electrical braking before the terminal. Around the route of the terminal station, the train is running on the unelectrified route, and the SOC of the battery pack becomes low. Afterwards, it gets charged again once returned to the electrified route. When the whole route is completed, the battery pack is charged high.

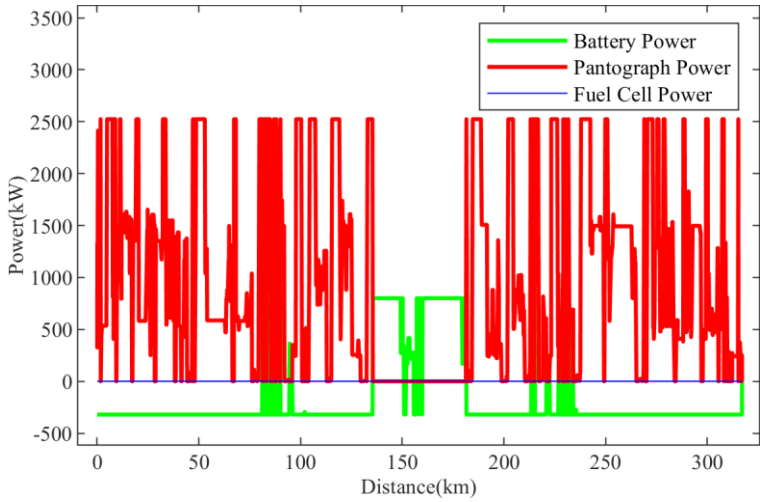

Fig. 15. Optimal train battery pack and pantograph power

TABLE V

OPTIMIZATION RESULTS

Train/route plan	Initial cost [£M]	Lifetime energy cost [£M]	Replacement cost [£M]	Time penalty [£M]	Fitness value [£M]	Cost saving
Benchmark diesel train	0	554.37	0	0	554.37	0
Hydrogen train	9.36	835.15	5.99	2.00	852.50	-53.78%
Full electrification (except tunnels)	275.92	143.29	0	0	419.20	24.38%
Full electrification	365.02	143.48	0	0	508.49	8.28%
Optimal train	194.02	160.47	1.87	4.56	360.92	34.90%

TABLE V shows the cost detail and fitness value for all scenarios. The HFC train has the lowest initial cost in the list of converted trains as there are no route rebuilding fees; it has a high energy cost because of the high price of hydrogen, although it uses less fuel energy than a diesel train. Moreover, the extra weight of the hydrogen fuel cell train produces its time penalty even with the same power output. Because of the lighter train bodyweight, the two full electrification scenarios take less time and are faster than the diesel trains. Although the train performance is almost the same, there is a considerable cost difference between the two electrification scenarios. From a cost point of view, train conversion cost and energy cost are nearly the same. However, investment in tunnel electrification is too expensive: 65.71% of the total cost of the route with no tunnel electrification is for electrification infrastructure; that percentage for full electrification including tunnels is even higher at 71.69%. The extra cost of tunnel electrification, extending the usual double-track route for another 25 km, is around £89 million. The route for the optimal train is still discontinuously electrification. Hence the initial cost is smaller than for full electrification. Also, its energy cost is not much higher than for the full electrification scenarios, so the total cost and fitness value are extremely low on the list. Hence, these three plans with electrification have a much higher initial cost, but the energy cost is relatively low, so that the total cost is less than for the hydrogen train.

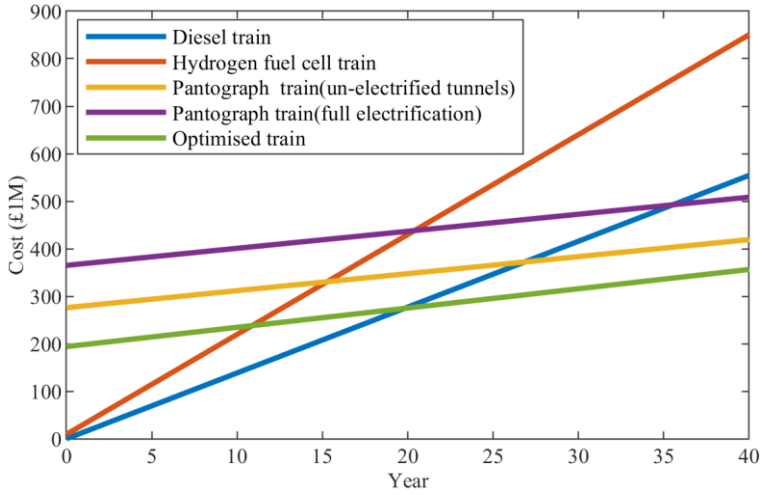

Fig. 16. Total cost without energy price change in 40 years

Fig. 16 shows the cost accumulation of the different scenarios over the entire 40 years. Calculating costs using current energy prices, the optimal train is the most economical after 20 years of operation. Diesel fuel is currently much cheaper than hydrogen, so that the annual operation cost, including energy and maintenance costs, for a diesel train is less than for an HFC train. The initial cost of investment in electrification is also too high, though the subsequent energy cost is much lower than a fuel train.

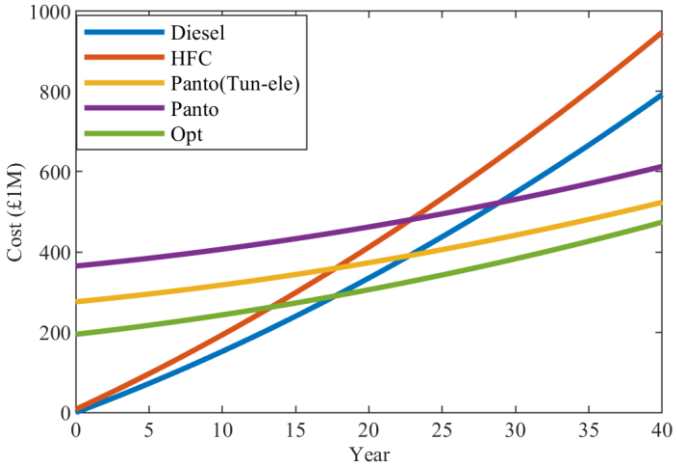

Fig. 17. Total cost with energy price changes in 40 years

TABLE VI

FINAL COST AFTER ENERGY PRICE CHANGES

Train	Final cost [£M]
Benchmark diesel train	792.19
Hydrogen train	1176.2
Full electrification (except tunnels)	522.59
Full electrification	612.02
Optimal train	472.14

From 1996 to 2020, diesel prices in the UK increased from £0.58 per liter to £1.25 per liter, whereas electricity prices rose about 6% per year since 2000 [42-44]. According to the prediction study, the hydrogen price has only increased by 2.2% each year since 2015 [45]. To unify the start year of each kind of energy price change rate, the energy base price is chosen from 2020. In this situation, diesel, electricity, and hydrogen price change rates are 2.2%, 3.7%, and 2%, respectively. After considering the fuel price change, the cost accumulation is shown in Fig. 17, and the estimated final cost of each scenario is listed in TABLE VI. Even hydrogen got the lowest energy rise during the following years; its final fitness value is exceptionally high, 19% higher than the benchmark diesel train. The main reason is that the base hydrogen fuel price limits HFC train financial-economic. According to the price prediction, the hydrogen fuel is £0.54 per kWh whereas diesel fuel is £0.24 per kWh after 40 years. Although electricity has a higher price increase rate, two scenarios with extended electrification did not profit less than before energy price changes due to low energy consumption. At the same time, the optimal train is still the best among those trains—40.4% less cost than diesel train.

D. Hydrogen fuel cells train future probability

The main reason why hydrogen fuel cell train does not get competitiveness is the high fuel price as further optimization under the hypothesis of lower hydrogen fuel price. If the current hydrogen price can be reduced to 74.07%, HFC can be considered to be installed in the optimal multi-mode train. Besides, once the price decreases by 29%, it can get a higher benefit than electrification. Therefore, the hydrogen fuel cell& battery pack train is more financially efficient.

V. CONCLUSIONS

This paper shows a method for converting the current diesel trains to multi-mode trains and rebuilding discontinuously electrified routes to minimize the total cost in the next 40 years in an environmentally friendly way within journey time requirements. An adaptive PSO algorithm is used to search for the optimal train conversion and route rebuilding plan depending on evaluating the fitness function value calculated by financial cost and journey time cost. A case study of Class 222 train conversion and route rebuilding from London St. Pancras to Leicester has been researched. Compared with the benchmark diesel train and other conversion or rebuilding scenarios in the case of fixed energy price, the optimal train conversion and route rebuilding plan cost 34.9% less than the environmentally harmful diesel train. After considering energy

price alterations, electric trains are more competitive in the case of low energy consumption, as fuel trains will incur a considerable increase in energy costs. The optimal train gets a higher cost reduction to 40.4%. Electrification of tunnels is too expensive compared with the regular route so that currently, there is no need to electrify short tunnels. If the hydrogen base price can decrease significantly, the HFC train can be competitive among those upgrading methods. In future work, other factors like traffic demand difference, headway difference, and traffic management will be considered to be discussed together as the optimization variables.

VI. REFERENCES

[1] C. Chéron, M. Walter, J. Sandor, and E. Wiebe, "European railway energy roadmap: towards 2030," 2011.

[2] J. Baker. "Will the UK ever get electrification back on track?," https://www.railway-technology.com/features/will-uk-ever-get-electrification-back-track/.

[3] "IMechE rail report backs hydrogen and electrification combination," https://www.theengineer.co.uk/imeche-report-hydrogen-electrification/.

[4] Z. Tian, N. Zhao, S. Hillmansen, C. Roberts, T. Dowens, and C. Kerr, "SmartDrive: Traction Energy Optimization and Applications in Rail Systems," *IEEE Transactions on Intelligent Transportation Systems*, vol. 20, no. 7, pp. 2764-2773, 2019.

[5] Z. Tian, S. Hillmansen, C. Roberts, P. Weston, N. Zhao, L. Chen, and M. Chen, "Energy evaluation of the power network of a DC railway system with regenerating trains," *IET Electrical Systems in Transportation*, vol. 6, no. 2, pp. 41-49, 2016.

[6] X. Zhao, B. Ke, and K. Lian, "Optimization of Train Speed Curve for Energy Saving Using Efficient and Accurate Electric Traction Models on the Mass Rapid Transit System," *IEEE Transactions on Transportation Electrification*, vol. 4, no. 4, pp. 922-935, 2018.

[7] D. Iannuzzi, and P. Tricoli, "Speed-Based State-of-Charge Tracking Control for Metro Trains With Onboard Supercapacitors," *IEEE Transactions on Power Electronics*, vol. 27, no. 4, pp. 2129-2140, 2012.

[8] K. Wang, H. Hu, J. Chen, J. Zhu, X. Zhong, and Z. He, "System-Level Dynamic Energy Consumption Evaluation for High-Speed Railway," *IEEE Transactions on Transportation Electrification*, vol. 5, no. 3, pp. 745-757, 2019.

[9] Z. Tian, P. Weston, N. Zhao, S. Hillmansen, C. Roberts, and L. Chen, "System energy optimisation strategies for metros with regeneration," *Transportation Research Part C: Emerging Technologies*, vol. 75, pp. 120-135, 2017.

[10] G. Zhang, Z. Tian, P. Tricoli, S. Hillmansen, Y. Wang, and Z. Liu, "Inverter Operating Characteristics Optimization for DC Traction Power Supply Systems," *IEEE Transactions on Vehicular Technology*, vol. 68, no. 4, pp. 3400-3410, 2019.

[11] J. Silmon, and S. Hillmansen, "Investigating discontinuous electrification and energy storage on the northern Trans-Pennine route." pp. 1-9.

[12] A. Hoffrichter, J. Silmon, F. Schmid, S. Hillmansen, and C. Roberts, "Feasibility of discontinuous electrification on the Great Western Main Line determined by train simulation," *Proceedings of the Institution of Mechanical Engineers*, pp. 11, 2013.

[13] M. A. Hannan, M. M. Hoque, A. Mohamed, and A. Ayob, "Review of energy storage systems for electric vehicle applications: Issues and challenges," *Renewable and Sustainable Energy Reviews*, vol. 69, pp. 771-789, 2017.

[14] Ş. İ, H. C. Kılıçkıran, H. Akdemir, B. Kekezo, gcaron, lu, O. Erdinç, and J. P. S. Catalão, "Energy Management of a Smart Railway Station Considering Regenerative Braking and Stochastic Behaviour of ESS and PV Generation," *IEEE Transactions on Sustainable Energy*, vol. 9, no. 3, pp. 1041-1050, 2018.

[15] J. A. Aguado, A. J. S. Racero, and S. d. l. Torre, "Optimal Operation of Electric Railways With Renewable Energy and Electric Storage Systems," *IEEE Transactions on Smart Grid*, vol. 9, no. 2, pp. 993-1001, 2018.

[16] C. Wu, W. Zhang, S. Lu, Z. Tan, F. Xue, and J. Yang, "Train Speed Trajectory Optimization With On-Board Energy Storage Device," *IEEE Transactions on Intelligent Transportation Systems*, vol. 20, no. 11, pp. 4092-4102, 2019.

[17] V. A. Kleftakis, and N. D. Hatziargyriou, "Optimal Control of Reversible Substations and Wayside Storage Devices for Voltage Stabilization and Energy Savings in Metro Railway Networks," *IEEE Transactions on Transportation Electrification*, vol. 5, no. 2, pp. 515-523, 2019.

[18] Z. Yang, Z. Yang, H. Xia, and F. Lin, "Brake Voltage Following Control of Supercapacitor-Based Energy Storage Systems in Metro Considering Train Operation State," *IEEE Transactions on Industrial Electronics*, vol. 65, no. 8, pp. 6751-6761, 2018.

[19] t. H. o. Commons, *Rail infrastructure investment: Government and Office of Rail and Road Responses to the Committee's Fourth Report*, 2018.

[20] A. Hoffrichter, S. Hillmansen, and C. Roberts, "Conceptual propulsion system design for a hydrogen-powered regional train," *IET Electrical Systems in Transportation*, vol. 6, no. 2, pp. 56-66, 2016.

[21] M. S. A. Chowdhury, K. A. A. Mamun, and A. M. Rahman, "Modelling and simulation of power system of battery, solar and fuel cell powered Hybrid Electric vehicle." pp. 1-6.

[22] T. Din, and S. Hillmansen, "Energy consumption and carbon dioxide emissions analysis for a concept design of a hydrogen hybrid railway vehicle," *IET Electrical Systems in Transportation*, vol. 8, no. 2, pp. 112-121, 2018.

[23] M. Walters, A. Kuhlmann, and J. Ogrzewalla, "Fuel cell range extender for battery electric vehicles." pp. 1-6.

[24] D. W. Gao, C. Mi, and A. Emadi, "Modeling and Simulation of Electric and Hybrid Vehicles," *Proceedings of the IEEE*, vol. 95, no. 4, pp. 729-745, 2007.

[25] A. S. Abdelrahman, Y. Attia, K. Woronowicz, and M. Z. Youssef, "Hybrid Fuel Cell/Battery Rail Car: A Feasibility Study," *IEEE Transactions on Transportation Electrification*, vol. 2, no. 4, pp. 493-503, 2016.

[26] Q. Li, B. Su, Y. Pu, Y. Han, T. Wang, L. Yin, and W. Chen, "A State Machine Control Based on Equivalent Consumption Minimization for Fuel Cell/ Supercapacitor Hybrid Tramway," *IEEE Transactions on Transportation Electrification*, vol. 5, no. 2, pp. 552-564, 2019.

[27] J. P. Torreglosa, P. García, L. M. Fernández, and F. Jurado, "Predictive Control for the Energy Management of a Fuel-Cell–Battery–Supercapacitor Tramway," *IEEE Transactions on Industrial Informatics*, vol. 10, no. 1, pp. 276-285, 2014.

[28] T. S. P. a. E. K. Scott F. Gorman, "The 'use-by date' for lithium-ion battery components," *Philosophical transactions of the royal society A*, 2019.

[29] X. Xu, Z. Li, and N. Chen, "A Hierarchical Model for Lithium-Ion Battery Degradation Prediction," *IEEE Transactions on Reliability*, vol. 65, no. 1, pp. 310-325, 2016.

[30] Y. Shi, and R. C. Eberhart, "Empirical study of particle swarm optimization." pp. 1945-1950 Vol. 3.

[31] M. Hu, T. Wu, and J. D. Weir, "An Adaptive Particle Swarm Optimization With Multiple Adaptive Methods," *IEEE Transactions on Evolutionary Computation*, vol. 17, no. 5, pp. 705-720, 2013.

[32] B. Son, J. Kim, J. Kim, Y. Kim, and S. Jung, "Adaptive Particle Swarm Optimization Based on Kernel Support Vector Machine for Optimal Design of Synchronous Reluctance Motor," *IEEE Transactions on Magnetics*, vol. 55, no. 6, pp. 1-5, 2019.

[33] Bridge, and Mike, *Railway Track Diagrams Book 4 Midlands & North West*, p.^pp. 1–5, 2013.

[34] Brailsford, and Martyn, *Railway Track Diagrams Book 2: Eastern*, 2016.

[35] B. E. AG. "EVB1 - HV - Battery (16 kWh / 400 V or 14 kWh / 350 V)," https://www.brusa.biz/_files/drive/05_Sales/Datasheets//BRUSA_DB_EN_EVB1.pdf.

[36] I. Perin, G. R. Walker, and G. Ledwich, "Load Sharing and Wayside Battery Storage for Improving AC Railway Network Performance With Generic Model for Capacity Estimation—Part 2," *IEEE Transactions on Industrial Electronics*, vol. 65, no. 12, pp. 9459-9467, 2018.
[37] *RIA Electrification Cost Challenge*, Railway Industry Association, 2019.
[38] D. S. Satyapal. "Hydrogen and Fuel Cells Overview," https://www.energy.gov/eere/fuelcells/downloads/hydrogen-and-fuel-cells-overview.
[39] L. Goldie-Scot. "A Behind the Scenes Take on Lithium-ion Battery Prices," https://about.bnef.com/blog/behind-scenes-take-lithium-ion-battery-prices/.
[40] B. Fan, C. Roberts, and P. Weston, "A comparison of algorithms for minimising delay costs in disturbed railway traffic scenarios," *Journal of Rail Transport Planning & Management*, vol. 2, no. 1, pp. 23-33, 2012/11/01/, 2012.
[41] B. FAN, "RAILWAY TRAFFIC RESCHEDULING APPROACHES TO MINIMISE DELAYS IN DISTURBED CONDITIONS," School of Electronic, Electrical and Computer Engineering, The University of Birmingham, 2012.
[42] "Wholesale Electricity Price Guide," https://www.businesselectricityprices.org.uk/retail-versus-wholesale-prices/.
[43] I. Tiseo. "Average price of diesel fuel in the United Kingdom (UK) from January 2015 and September 2019 (in pence per liter)," https://www.statista.com/statistics/299552/average-price-of-diesel-in-the-united-kingdom/.
[44] M. Grubb, and P. Drummond, "UK Industrial Electricity Prices: Competitiveness in a low carbon world," 2018.
[45] A. Abad, R. Steinberger-Wilckens, J. Radcliffe, N. A. Al-Mufachi, P. Dodds, O. Jones, and Z. Kurban, *The role of Hydrogen and Fuel Cells in delivering Energy Security for the UK*, 2017.